PAPER

Optimization of an artificial neural network to estimate laser ablation efficiency

IOP Publishing | Astro Ltd Laser Physics

Laser Phys. **29** (2019) 115603 (7pp) https://doi.org/10.1088/1555-6611/ab43d9

Optimization of an artificial neural network to estimate laser ablation efficiency

Fikret Yildiz

Faculty of Engineering, Electrical and Electronics Department, Hakkari University, 3000, Hakkari, Turkey

E-mail: fikretyildiz@hakkari.edu.tr

Received 17 July 2019
Accepted for publication 10 September 2019
Published 2 October 2019

Abstract

The use of fiber laser in surgery has many advantages due to its small size, efficiency, operation in continuous and pulse mode and easy coupling to fiber optics for various applications. Laser surgery requires very precise control on laser parameters, and imprecision can cause unacceptable damages during operation, particularly in neurosurgical applications. There have been many experimental studies looking to optimize laser parameters to control laser thermal therapy. In this study, we propose an artificial neural network method (ANN) to predict laser ablation damage as a function of laser parameters and temperature. The purpose of this study was to investigate the performance of artificial neural networks to predict the ablation efficiency of a 1940 nm thulium fiber laser on ovine brain tissue. Twelve experimental data were used to train an ANN model. Tissue type (cortical/subcortical), laser mode, laser power, laser energy, time, temperature and temperature change were used as inputs for the ANN and the ablation efficiency (ablated area/total thermally altered area) was the output of the model. Four untrained data were used to validate the ANN prediction ability after finding correlation between the ANN inputs and output. Experimental and predicted data were compared to find the accuracy of the model. Moreover, optimum laser mode (continuous/pulse) selection was also studied. Five different machine learning methods were used for laser mode selection, and the results were compared. Our results showed that prediction for the ablation efficiency of an ANN is lower than 15% and 87.5% classification accuracy was obtained for optimum laser mode selection.

Keywords: laser ablation, thulium fiber laser, artificial neural network (ANN), machine learning, neurosurgery

(Some figures may appear in colour only in the online journal)

1. Introduction

Ablative techniques, both thermal and non-thermal, have been used in therapeutic applications in a wide variety of medical areas [1–5]. As an alternative to surgery, they are gaining increasing interest due to not only their focal destruction of a target with sparing collateral normal tissue, but the way in which they are also capable of lower physical impact, pain, trauma, and a reduction in the overall intervention cost and recovery time [5–9]. Among ablative techniques, laser ablation (LA) has great capability of guiding a laser beam into tumors through a highly efficient and small sized flexible fiber, with cell death being induced by the principle of conversion of absorbed laser light to heat [10, 11]. Coagulation, vaporization, carbonization and melting of target tissue are the direct effects of thermal energy, as illustrated in figure 1. These are observed at the temperature ranges of 50 °C–60 °C, 100 °C–300 °C and >300 °C, respectively [12, 13]. Advantages of thin and flexible laser fibers are that they make it possible to reach tumors more easily and safely [11, 14]. Moreover, a fiber with multiple outputs enables the treatment of lesions that are different in size, without damaging surrounding healthy tissue as far as possible [5, 11]. The mechanism of light energy to heat conversion has been proposed to treat brain cancer, and the liver, pancreas, kidneys, thyroid and prostate, using different laser sources [15–19]. Laser parameters (wavelength, laser power, laser energy, application time and laser mode), the physical properties of the tissue, and the fiber type are

mainly responsible for heat generation [4, 9, 20]. Proper selection of these parameters has become an important issue for accurate treatment, with the elimination of undesired thermal effects on normal tissue. Therefore, various lasers have been used to treat tumors, which are placed at different depths of organs. When a target is in deep-lying organs, Nd:YAG lasers (1064 nm), diode lasers (800–900 nm) and KTP:YAG lasers (532 nm) would be good ablation systems, due to poor absorption by water in the infrared region [9, 21–24]. In contrast, water absorption reaches its peak value around 3 μm or 2 μm and laser wavelengths around these regions have the ability to ablate soft tissues while providing minimum side effects on healthy tissue. For example, CO_2 (10 600 nm), Thulium (2016 nm) and Er:YAG (2940 nm) have been reported in the literature as superficial tissue ablation systems [9, 21–25].

However, one of the most significant drawbacks of those systems is the transfer of laser energy through silica fiber. Silica fibers are cheap and easy to use, however they are not suitable for the transfer of laser wavelengths longer than 2 μm [23]. Therefore, a Thulium fiber laser was introduced as an alternative and is an attractive choice for different applications. Recently, performances of a 1940 nm Thulium fiber laser have been shown for neurosurgical applications, liver tissue ablation, intraoral surgery, ceramic bracket debonding, tissue welding, etc [24, 26–28]. Tight control of the laser parameters and induced temperature are frequently mentioned as the limitations of a laser ablation system [8]. Laser surgery requires very precise control on laser parameters, and imprecision can cause unacceptable damage during operation. Because excessive temperature increase results in evaporation, when the target area temperature is raised more than the threshold value, undesired carbonization occurs [8].

There are many invasive and non-invasive accurate tissue temperature monitoring systems used in laser application to tissue. The most promising invasive techniques use thermistors, thermocouples and fiber optic-based sensors. They have good spatial resolution, and quite good accuracy for real-time temperature monitoring. MRI and CT can provide temperature variation estimations in near-real time, but have some disadvantages, including the high cost of operation and ionizing radiation [8, 9, 24, 25, 29, 30]. The use of an optimum laser ablation system has therefore been under investigation. To refer to the above studies, it is clear that further attempts are required to find the optimum laser wavelength and temperature monitoring system for reliable laser ablation operation. It has been mentioned that there is no linear relation between laser settings and tissue temperature increase [31]. Hence, cell death is generally estimated using a complex mathematical analysis, based on Arrhenius rate analysis [32]. Considering the many laser and tissue parameters that exist, it is not an easy task to use experimental and theoretical methods to find the relationship between these parameters in order to control laser-induced ablation. There are intensive experimental and analytical works to discover the correlations between laser parameters and induced thermal damages.

Moreover, there is an easier, more functional, and time and cost saving method, which is an artificial neural network (ANN). When the relation between input and output variables

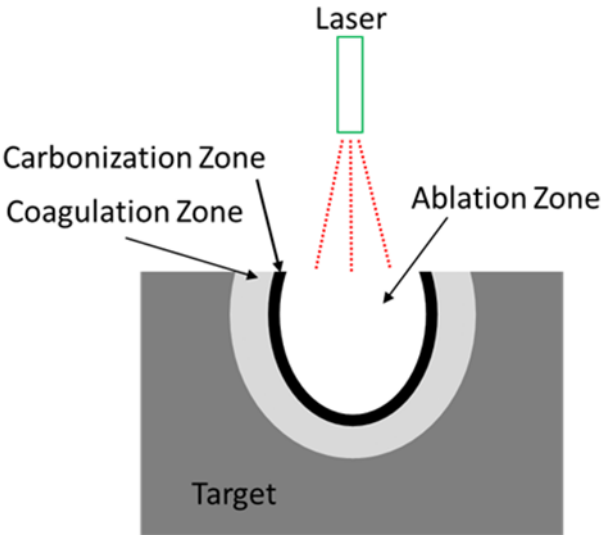

Figure 1. Illustration of three different laser-induced thermal damages on target tissue.

is not fully understood and analytical models lack reliability, an ANN can give us reasonable results [33]. This is because ANNs have the capability to manage dynamic and complex processes with high accuracy. For modeling complex and nonlinear systems, ANNs are accepted as unevitable classifier and prediction tools. Short installation time and low cost are other advantages of ANNs. An ANN would therefore be a good choice for laser-induced thermal damage estimation as a function of a different number of input parameters [34].

Use of industrial lasers with an ANN has been extensively studied for different applications. Controlling the laser power, scan speed, pulse duration, and pulse frequency using an ANN can provide precise 3D material processing [35]. An ANN can optimize laser inputs, such as the gas pressure ratio and discharge current, and obtain maximum output power. It has also been shown that an ANN can test laser thermoplastic weld quality using an estimated correlation between the inputs (laser power, welding speed, stand-off distance and clamping pressure) and outputs (lap-shear strength and weld-seam width) [33].

For ANN-assisted medical laser applications, a limited number of studies in the literature can be found for laser ablation treatment. One recent study showed that the diameter and depth of ablation were estimated with an ANN by using power and application time as inputs. However, the laser ablation process depends on more laser parameters (such as temperature change) rather than on time and power [36]. Another work used an ANN to predict the effect of three different laser sources, 980 nm, 1070 nm and 1940 nm, on the induced coagulation diameter and depth on liver tissue. Application time, power, spot size, penetration depth and wavelength were used as the ANN inputs to estimate these. It was found that an ANN can estimate laser induced thermal damage with limited number of experimental data. The ANN results were compared with mathematical models to show the superior prediction ability of the ANN [34, 37]. As shown in previous studies, prediction of laser-induced thermal damage and laser parameters

selection using ANN can pave the way for safer and more precise laser ablation treatment for both operators and patients. This is because, when an ANN can learn the relation between laser parameters and induced damages, we can easily set the laser parameters with a known output (thermal damage) and finish operation with minimum tissue damage on surrounding healthy tissue.

In this study, a feed forward ANN model with Levenberg–Marquardt (LM) algorithms was developed in order to estimate laser ablation efficiency (AE) (diameter of ablation zone/total thermally altered zone) and find the optimum laser mode selection. The data used in this study were obtained from recently presented experimental data of a 1940 nm Thulium fiber application on an ovine brain [24]. This laser ablation system consisted of a continuous mode 1940 nm Thulium fiber laser and real time thermocouple measurement systems. Tissue type (cortical/subcortical), laser mode, laser power, laser energy, exposure time, temperature and temperature change are the inputs of the ANN. Among the 16 experimental data of cortical and subcortical tissue, 12 were selected for the training network and the rest were chosen for validating the trained network. The number of hidden layers, learning rate, momentum constant and number of iterations were optimized beforehand, to test the ANN model performance in terms of prediction of AE and laser mode selection. Finally, it was found that the ANN can estimate AE with a minimum accuracy 2.1%, and find the optimum laser mode with a 87.5% success rate.

2. Materials and methods

In our study, data were obtained from previously published works [24, 28]. In this study a CW mode 1940 nm Thulium fiber laser (TLR-5-1940;IPG Laser GmbH, Germany) was used with a maximum power of 5 W. Laser parameters such as output power, laser mode (continuous or pulse), and application time were controlled by a custom built controller unit (Teknofil, Inc., Istanbul, Turkey) and the user easily accessed the parameters via a user-friendly LabView interface. Laser light was transferred to the ovina brain tissues through a 1 m cable and coupled to a 400 μm fiber (NA:0.39) using focusing lenses and xyz alignment apparatus. The output dose of the laser source was confirmed before each experimental trial using an optical power meter (Newport 1918-C, Irvine, CA). A 1940 nm Tm:Fiber laser was applied in the vertical direction on the cortical and subcortical part of the ovina tissues. The distance between the fiber end and tissue surface was 0–0.2 mm. The distal end of the fiber was always checked before each application to prevent irregularities (breaks, or carbonization) at the fiber tip. In order to determine the laser application parameters, a pre-dosimetry study was conducted. Coagulation and carbonization onset time were recorded for various applications of power, ranging from 200 mW to 1400 mW. It was confirmed that a laser power of more than 800 mW caused carbonization, and thus maximum application power was set 800 mW. Laser application time and pulse width were selected to deliver the same amount of energy (2 J and 4 J). A

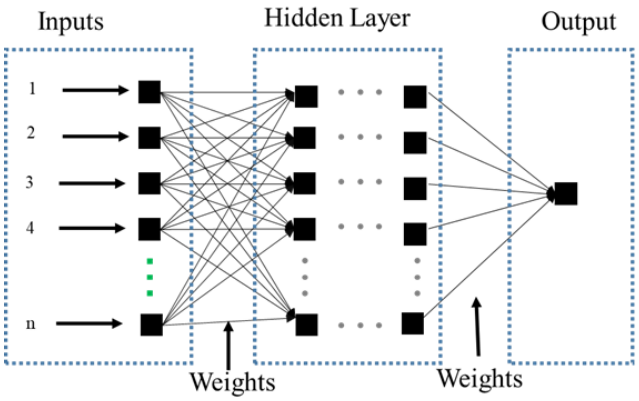

Figure 2. Structure of the ANN.

k-type thermocouple was used for temperature measurement during laser application. The number of experimental data for each tissue type was 16. The experimental data is given in [24]. Ablated and coagulated tissue dimensions (the thermally altered area) were observed under a light microscope to calculate the AE of the laser with different application conditions. Further detail on the experimentation and data collection can be found in the previously reported study [24, 28].

Following data collection, an ANN structure was formed. This part of the study includes three steps. An ANN mimics the human neural system and consists of an input layer, hidden layers and an output layer, as illustrated in figure 2. These layers are connected to each other through weights, and an ANN trains the network by finding the best relation between these layers by changing the weight iteratively, until the optimum values are reached. The number of hidden layers, learning rate (*lr*), number of iterations and momentum constant (*mc*) are the critical parameters of an ANN structure, because they affect the ANN success rate. Thus, the initial step is to find the best ANN structure by optimizing the ANN parameters. The first task is data normalization. To do this, experimental data was normalized between 0–1. Data was divided into two sets: training-testing (75%) and validation (25%). Among the 16 experimental data, 12 were selected for the training-testing network and the rest (4) were chosen for validation the trained network.

After normalization, the k-fold cross validation method was applied to obtain the training and test data. Data was divided into sub-groups using k-fold cross validation. This method requires us to use all the data points in the data as training and test data. If we consider K:10, data was divided into ten separate datasets. In the first run, one of the ten datasets were used as training and the remaining nine datasets were testing. At the second run, two of ten datasets were used as training and the remaining nine datasets were used for testing. This process continues until the point is reached where all data has been used as both training and testing.

Lastly, the ANN architectures were optimized in terms of the number of hidden layers, learning rate (*lr*), number of iterations and momentum constant (*mc*) following k-fold cross validation. To find the optimum parameters of the ANN, the process was as follows. (1) The number of hidden layers was

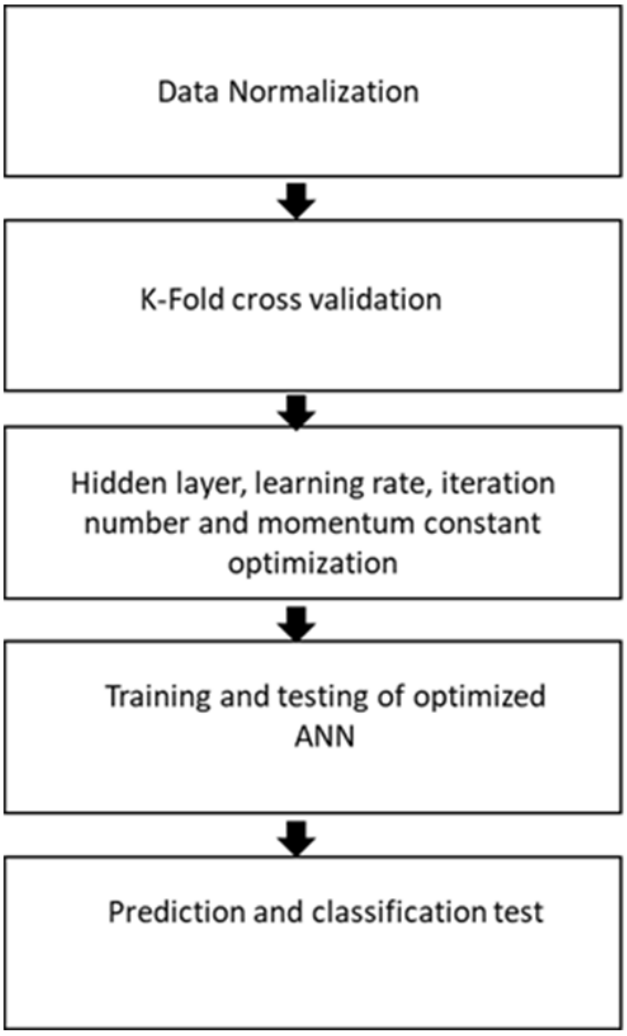

Figure 3. Workflow of the ANN optimization and performance analysis of the optimized ANN.

changed from 2 to 100, and the remaining parameters were kept constant until the highest test accuracy of mean square error (MSE), root mean square error (RMSE), mean absolute error (MAE) and ROUND function were found. The ROUND function rounds the data to the closest integer number. (2) The learning rate (*lr*) was changed from 0.1 to 5 and the remaining parameters with the optimum number of hidden layers were kept constant until the highest test accuracy of the MSE, RMSE, MAE and ROUND function were found. (3) The momentum constant (*mc*) was changed from 0.1 to 1 and the remaining parameters with the optimum number of hidden layer and learning rate (*lr*) were kept constant until the highest test accuracy of the MSE, RMSE, MAE and ROUND function were found. (4) The number of iterations was changed from 100 to 1000 and the remaining parameters with the optimum number of hidden layer momentum constant (*mc*) and learning rate (*lr*) were kept constant until highest test accuracy of the MSE, RMSE, MAE and ROUND function were found. The learning algorithm and activation functions used in the ANN were the LM backpropagation algorithm and sigmoid function, respectively. The ANN optimization process flow and performance testing steps of the optimized ANN are

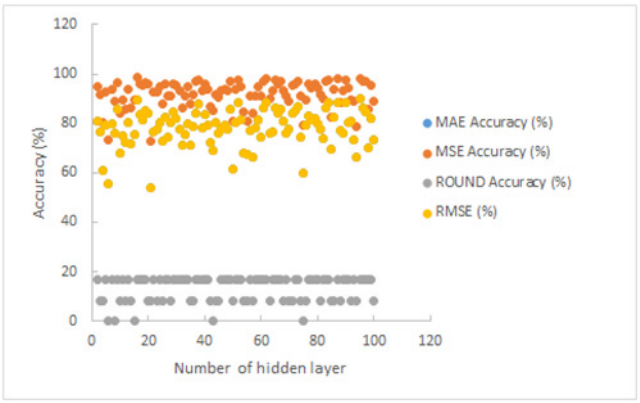

Figure 4. Error accuracy of the ANN as a function of hidden layers for cortical tissue.

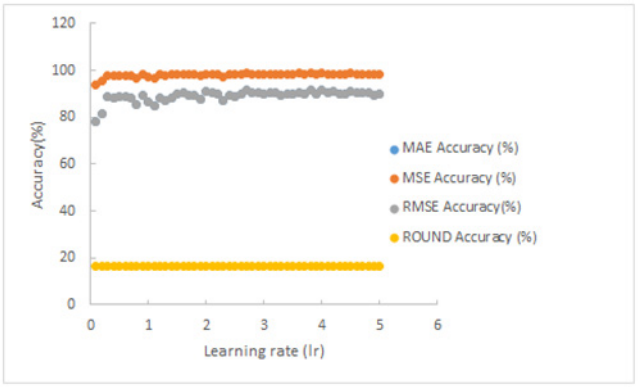

Figure 5. Learning rate optimization results in terms of the MAE, MSE, RMSE and ROUND function accuracy.

summarized in figure 3. The MSE was used to find the optimized parameters of the ANN due to higher accuracy than the RMSE, MAE and ROUND function, as shown in figure 4.

3. Results and discussion

This study mainly focused on an investigation of ANN prediction ability in terms of a 1940 nm Tm:Fiber laser-induced AE on ovina brain tissue. In addition to prediction ability, laser mode selection for given laser parameters and tissue types was also studied to show the ANN classification success.

3.1. ANN prediction performance

A 1940 nm Tm:fiber laser was applied on two different tissues: the cortical and subcortical part of an ovina brain. Therefore, the ANN structures for these two different tissues were evaluated separately. The optimization results of the ANN structure were obtained separately for cortical and subcortical tissue. Test data accuracy of the MSE, RMSE, MAE and ROUND function error were compared and contrasted to find the optimum values of hidden layers, learning rate (*lr*), momentum constant (*mc*) and number of iterations. Test data accuracy of the MSE, RMSE, MAE and ROUND function are shown in figures 4 and 5 as a function of the number of hidden layers and learning rate for cortical tissue. These figures show that MSE has

Table 1. Parameters of the optimum ANN structure.

Parameters	Tissue type	
	Subcortical	Cortical
No. of neurons in input layer	6	6
No. of neurons in output layer	1	1
No. of hidden layers	71	16
Training functions	LM	LM
Performance accuracy	MSE (%98.8)	MSE (%98.4)
Activation function	Log-sigmoid	Log-sigmoid
Maximum epoch	800	200
Learning rate (*lr*)	0.4	3.8
Momentum constant (*mc*)	0.1	0.1
Performance goal	0	0

the highest test accuracy for both hidden layers and learning rate (*lr*) for cortical tissue. The same results were obtained for the number of iterations and momentum constant (*mc*). It was found that RMSE and MAE have the same error accuracy, and the ROUND function has the lowest accuracy, as shown in figures 4 and 5. The MSE also showed the best performance compared with the others for determining the optimum ANN parameters for subcortical tissue data. Therefore, the comparison of MSE results was used to find the optimum number of hidden layers, learning rate (*lr*), number of iterations and momentum constant (*mc*). The optimized ANN parameters are summarized in table 1. A total of 4 unexposed data of 16 were applied by the ANN to predict the AE of the 1940 nm Tm:Fiber laser following the ANN optimization process. The optimum structure of the ANN was 6-71-1 and 6-16-1 for the subcortical and cortical tissue, respectively, as described in table 1. A comparison of experimental (actual) and predicted data of AE is summarized in table 2. In this table, LM, *P*, LE, *t*, *T*, ($\Delta T/t$) and AE describe the laser mode, power, laser energy, time, temperature, temperature change, and ablation efficiency, respectively. The laser mode '0' means a continuous mode, and '1' equals a pulsed modulated mode of the laser. The relationship between the actual and predicted data was evaluated with a value of correlation coefficient (R^2). A linear regression between the actual and predicted data was observed. The values of the correlation coefficient (R^2) were 0.9403 and 0.9951 for subcortical and cortical tissue data, respectively. The maximum prediction error of AE between the experimental and predicted data was found to be 15% for subcortical tissue. For cortical tissue, the maximum prediction error was 23%. More accurate results were obtained in the case of a minimum of 2.1% and 4.6% prediction error for cortical and subcortical tissue sample, respectively. The prediction error of the optimized ANN model we used in this study is between 4.6% and 15% for subcortical tissue. Additionally, the maximum and minimum prediction errors for cortical tissue are 2.1% to 23%. In the previous study, the maximum prediction error of ANN for the coagulation diameter was 34.36% and a 22.4% error between actual and predicted data was found for the coagulation depth estimation. Our results proved that laser AE can be estimated more precisely than coagulated tissue damage. It is also possible that using different learning algorithms to LM, which is used in this study, may improve the optimized ANN results for AE estimation.

3.2. Classification performance

It has been mentioned that the thermal effects of laser light on tissue depend on the laser parameters (operation mode and wavelength) [9]. Laser is applied in two modes: a continuous mode with lower power and long application time, and pulse mode, where high power is applied intermittently to the target. The amount of damaged volume due to temperature change is not a linear function with respect to the laser settings [9, 31, 38]. Therefore, laser mode selection is an important parameter for precise ablation process control and results. Knowing which laser mode is suitable for a given tissue and the laser parameters with the help of the ANN classification ability has also been investigated. To determine the optimum laser mode selection, data, which was used for prediction, was rearranged. AE was replaced by laser mode as an output and AE is accepted as one of the inputs. The remaining inputs of ANN, P, LE, t, T, and (ΔT/t), were kept the same. The Weka 3. software program was used to show the laser mode selection

$$\text{TP rate} = \frac{\text{TP}}{\text{TP} + \text{FN}} \tag{1}$$

$$\text{FP rate} = \frac{\text{FP}}{\text{FP} + \text{TN}} \tag{2}$$

$$\text{Prc} = \frac{\text{TP}}{\text{TP} + \text{FP}} \tag{3}$$

$$\text{F} = 2 * \frac{\text{Prc} * \text{TP rate}}{\text{Prc} + \text{Tp rate}} \tag{4}$$

$$\text{MCC} = \frac{(\text{TP} * \text{TN}) - (\text{FP} * \text{FN})}{\sqrt{(\text{TP} + \text{FP})(\text{TP} + \text{FN})(\text{TN} + \text{FP})(\text{TN} + \text{FN})}} \tag{5}$$

$$\text{ACC} = \frac{(\text{Correctly classified instances})}{(\text{Total number of intances})} * 100 \tag{6}$$

ability of ANN classifier [39]. The success of the system was determined with a confusion matrix, as seen in table 4. Four different machine learning algorithms (classifiers) of the Weka 3.8 software program were employed in this work to compare the success rates with the ANN system. These classifiers are a support vector machine (SVM), Naive Bayes (NB), random forest (RF), and decision tree (DT). The performances of the machine learning techniques were compared in terms of the most commonly used parameters: (a) precision (Prc), (b) TP rate, (c) FP rate, (d) F measure (F) , and (e) the Matthews correlation coefficient (MCC). These parameters have a binary value between 0 and 1. The classifier performance is best (100%) when all four parameters (Prc, TP rate, F and MCC) have a value of '1'. The classifier performance is worst with a value of '0'. [40]. The TP rate, FP rate, Prc, F and MCC value were obtained using equations [41, equations (1)–(5)]. More information can be found in some of recent studies [42–44]. The first possibility is true positive (TP); in this case, the laser is in pulse mode (1) and the algorithm detects it correctly. The second case, true negative (TN), indicates that the continuous (0) mode of laser is determined correctly. The third case refers

Table 2. Prediction results of AE using the ANN.

LM	P (mW)	LE (J)	t (sn)	ΔT (°C)	$\Delta T/t$ (°C sn^{-1})	Experimental_AE (%)	Predicted_AE (%)	Absolute error (%)
				Subcortical tissue				
0	200	2	17,2	12,5	0,72	33,16	38,2	**15,4**
1	400	2	14,7	12,36	0,84	35,1	36,7	**4,6**
1	600	4	18,8	25,48	1,35	44,14	40,8	**7,5**
0	800	4	9,1	32,6	3,58	56,35	47,8	**15,0**
				Cortical tissue				
0	200	2	15,4	9,1	0,59	40,95	47,2	**15,4**
1	400	2	12,7	9,1	0,71	37,91	46,6	**23,0**
0	600	4	8,7	18,3	2,10	65,2	63,2	**2,9**
1	800	4	12,1	39,86	3,29	61,56	60,2	**2,1**

Table 3. Performance evaluation of five different machine learning algorithms: artificial neural network (ANN), support vector machine (SVM), Naive Bayes (NB), random forest (RF) and decision tree (DT). TNI: total number of instances and CCI: correctly classified instances.

Classifier	TNI	CCI	TP rate	FP rate	Prc	F	MCC	Kappa	ACC (%)
ANN	32	28	0.87	0.12	0.87	0.87	0.74	0.74	**87.5**
SVM	32	23	0.71	0.28	0.72	0.71	0.44	0.43	**71.8**
NB	32	21	0.65	0.34	0.65	0.65	0.31	0.31	**65.6**
RF	32	20	0.62	0.37	0.62	0.62	0.25	0.25	**62.5**
DT	32	18	0.56	0.43	0.56	0.56	0.12	0.12	**56.2**

Table 4. Confusion matrix.

		Actual values	
		Positive (1)	Negative (0)
Predicted values	Positive (1)	TP	FP
	Negative (0)	FN	TN

to false positive (FP), and in this case, the laser mode is continuous (0), however, the system gives pulse mode (1) output. This refers to incorrect classification. In the case of false negative (FN), the laser mode is in pulse mode (1), however, the system gives continuous mode (0) output incorrectly.

There are two more parameters to be considered to evaluate the machine learning algorithms in addition to Prc, TP rate, F and MCC. The first is Cohen's kappa coefficient, which was used to measure agreement between raters. This coefficient is expressed as almost perfect agreement in the range of 0.81–1.

The average accuracy rate (ACC) of the classification process is the second of these remaining parameters, and was calculated using equation (6) [40]. Comparisons of the five machine learning algorithms' accuracy performances in terms of Prc, TP rate, FP rate, F measure, MCC and kappa coefficient are shown in table 3. A total of 32 data were used for classification, and the data were normalized and subjected to the 10-fold cross validation technique before the classifier was run. The default setting was used for each classifier. Our results showed that the ANN algorithm gives maximum accuracy with a value of 87.5%. Moreover, the kappa coefficient of the ANN (0.74) is very close to the range of 0.81–1, as explained above. The SVM algorithm accuracy performance is also promising and satisfactory. The SVM produces 71.8% classification accuracy in this work. When compared to the ANN and SVM algorithms, the NB, RT and DT algorithm accuracy performance is lower. DT has the worst classifier compared to the others due to 56.2% accuracy. It was confirmed that laser mode selection is also determined when the desired laser parameters and AE are given as input to the ANN. These results show that ANN classification ability can provide safer tissue ablation, by helping to find the optimum laser mode selection.

4. Conclusion

The aim of this study was to investigate the prediction of AE induced by a 1940 nm Tm:fiber laser on an ovine brain using an ANN. The ANN prediction performance was shown separately on cortical and subcortical brain tissue. The study showed promising results that AE on cortical and subcortical brain tissue can be estimated with a maximum error of 15% and 23%, respectively. Furthermore, the optimum laser mode selection was also studied using the classification ability of the ANN. It was also confirmed that the optimum laser mode selection can be obtained by an ANN with 87.5% accuracy under a limited number of data. Therefore, we can say that an ANN can be used in intensive experimental and analytical works to more easily find the correlation between laser parameters and induced thermal damage, and eliminate the loss of time and high cost. Moreover, an ANN can assist a more unexperienced operator by checking and comparing the laser application parameters with the desired laser ablation damage before an operation, to prevent unacceptable results.

As a conclusion, an ANN-assisted laser ablation system can provide more accurate, reliable, safe and precise operation when considering tumor ablation on critical organs.

References

[1] Carrafiello G *et al* 2008 Microwave tumors ablation: principles, clinical applications and review of preliminary experiences *Int. J. Surg.* **6** 65–9

[2] Puggioni A, Kalra M, Carmo M, Mozes G and Gloviczki P 2005 Endovenous laser therapy and radiofrequency ablation of the great saphenous vein: analysis of early efficacy and complications *J. Vasc. Surg.* **42** 488–93

[3] Sartori S, Di Vece F, Ermili F and Tombesi P 2017 Laser ablation of liver tumors: An ancillary technique, or an alternative to radiofrequency and microwave? *World J. Radiol.* **9** 91

[4] Sartori S, Tombesi P and Di Vece F 2015 Radiofrequency, microwave, and laser ablation of liver tumors: time to move toward a tailored ablation technique? *Hepatoma Res.* **1** 52

[5] Wu J (ed) 2013 *Technological Advancements in Biomedicine for Healthcare Applications* (Hershey, PA: IGI Global)

[6] Proctor M R 2005 *Minimally Invasive Neurosurgery* (Berlin: Springer)

[7] Vog T,Mack M G, Straub R, Engelmann K, Zangos S and Woitazek D 2001 MR guided laser-induced thermotherapy (LITT) of malignant liver and soft tissue tumours *Med. Laser Appl.* **16** 91–102

[8] Gassino R, Liu Y, Konstantaki M, Vallan A, Pissadakis S and Perrone G 2017 A fiber optic probe for tumor laser ablation with integrated temperature measurement capability *J. Light. Technol.* **35** 3447–54

[9] Schena E, Saccomandi P and Fong Y 2017 Laser ablation for cancer: past, present and future *J. Funct. Biomater.* **8** 19

[10] Walser E M 2005 Percutaneous laser ablation in the treatment of hepatocellular carcinoma with a tumor size of 4 cm or smaller : analysis of factors affecting the achievement of tumor necrosis *J. Vasc. Interv. Radiol.* **16** 1427–9

[11] Pacella C M *et al* 2005 Percutaneous laser ablation in the treatment of hepatocellular carcinoma with small tumors: analysis of factors affecting the achievement of tumor necrosis *J. Vasc. Interv. Radiol.* **16** 1447–57

[12] Peng Q *et al* 2008 Lasers in medicine *Rep. Prog. Phys.* **71** 056701

[13] Niemz M H 2007 *Lasers-Tissue Interactions: Fundamentals and Applications* 3rd edn (Berlin: Springer)

[14] Pacella C M, Francica G, Giuseppe G and Costanzo D 2011 Laser ablation for small hepatocellular carcinoma *Radiol. Res. Prac.* **2011** 595627

[15] Tombesi P, Di Vece F and Sartori S 2015 Laser ablation for hepatic metastases from neuroendocrine tumors *Am. J. Roentgenol.* **204** W732

[16] Di Matteo F *et al* 2013 US-guided application of Nd:YAG laser in porcine pancreatic tissue: An *ex vivo* study and numerical simulation *Gastrointest. Endosc.* **78** 750–5

[17] Ritz J P *et al* 2011 Effectiveness of various thermal ablation techniques for the treatment of nodular thyroid disease—comparison of laser-induced thermotherapy and bipolar radiofrequency ablation *Lasers Med. Sci.* **26** 545–52

[18] Wu X *et al* 2018 Theoretical and experimental study of dual-fiber laser ablation for prostate cancer *PLoS One* **13** 1–13

[19] Belykh E *et al* 2017 Laser application in neurosurgery *Surg. Neurol. Int.* **8** 1–7

[20] Muller G J and Roggan A 1995 *Laser-Induced Interstitial Thermotherapy* (Bellingham, WA: SPIE)

[21] Welch A J, Motamedi M, Rastegar S, LeCarpentier G L and Jansen D 1991 Laser thermal ablation 1991 *Photochem. Photobiol.* **53** 815–23

[22] Jacques S L 2013 Optical properties of biological tissues: a review *Phys. Med. Biol.* **58**
Jacques S L 2013 Optical properties of biological tissues: a review *Phys. Med. Biol.* **58** 5007–8 (erratum)

[23] Bilici T, Tabakoglu Ö, Kalaycioglu H, Kurt A, Sennaroglu A and Gülsoy M 2009 Modulated and continuous-wave operations of Thulium (Tm:YAP) laser in tissue welding *Pacific Rim Conf. Lasers Electro-Optics, CLEO—Technical Digest (June 2010)* vol 15, pp 1–9

[24] Tunc B and Gulsoy M 2013 Tm: fiber laser ablation with real-time temperature monitoring for minimizing collateral thermal damage: *ex vivo* dosimetry for ovine brain *Laser Surg. Med.* **56** 48–56

[25] Alagha H Z, Alagha H Z and Gülsoy M 2019 Photothermal ablation of liver tissue with 1940-nm thulium fiber laser : an *ex vivo* study on lamb liver thulium fiber laser : an *ex vivo* study on lamb liver *J. Biomed. Opt.* **21** 1

[26] Sarp A S K and Gülsoy M 2011 Ceramic bracket debonding with ytterbium fiber laser *Lasers Med. Sci.* **26** 577–84

[27] Guney M, Tunc B and Gulsoy M 2014 Investigating the ablation efficiency of a 1940-nm thulium fibre laser for intraoral surgery *Int. J. Oral Maxillofac. Surg.* **43** 1015–21

[28] Tunc B and Gulsoy M 2014 Stereotaxic laser brain surgery with 1940-nm Tm : fiber laser: an *in vivo* study *Laser Surg. Med.* **51** 643–52

[29] Schena E *et al* 2013 Experimental assessment of CT-based thermometry during laser ablation of porcine pancreas *Phys. Med. Biol.* **58** 5705–16

[30] Saccomandi P, Schena E and Silvestri S 2013 Techniques for temperature monitoring during laser-induced thermotherapy: an overview *Int. J. Hyperth.* **29** 609–19

[31] Saccomandi P *et al* 2012 Theoretical analysis and experimental evaluation of laser-induced interstitial thermotherapy in *ex vivo* porcine pancreas *IEEE Trans. Biomed. Eng.* **59** 2958–64

[32] Stafford K, Fuentes R J, Elliott D, Weinberg A A and Ahrar J S 2010 Laser-induced thermal therapy for tumor ablation *Crit. Rev. Biomed. Eng.* **39** 79–100

[33] Acherjee B, Mondal S, Tudu B and Misra D 2011 Application of artificial neural network for predicting weld quality in laser transmission welding of thermoplastics *Appl. Soft Comput. J.* **11** 2548–55

[34] Yildiz F and Özdemir A T 2019 Prediction of laser-induced thermal damage with artificial neural networks *Laser Phys.* **29** 075205

[35] Campanelli S L, Casalino G, Ludovico A D and Bonserio C 2013 An artificial neural network approach for the control of the laser milling process *Int. J. Adv. Manuf. Technol.* **66** 1777–84

[36] Su B, Tang J and Liao H 2015 Automatic laser ablation control algorithm for an novel endoscopic laser ablation end effector for precision neurosurgery *IEEE Int. Conf. Intelligent Robots and Systems (December 2015)* pp 4362–7

[37] Yildiz F, Gulsoy M and Cilesiz I 2016 An experimental study on photothermal damage to tissue: the role of irradiance and wavelength *Laser Phys.* **26** 095601

[38] Nikfarjam M and Christophi C 2003 Interstitial laser thermotherapy for liver tumours *Br. J. Surg.* **90** 1033–47

[39] Witten I H, Frank E, Trigg L E, Hall M A, Holmes G and Cunningham S J 1999 Weka: Practical machine learning tools and techniques with Java implementations *Working Paper Series* **99** 1–5

[40] Yücelbas S, Yücelbas C, Tezel G, Özsen S, Küççüktürk S and Yosunkaya S 2017 Pre-determination of OSA degree using morphological features of the ECG signal *Expert Syst. Appl.* **81** 79–87

[41] Ma Y, Guo L and Cukic B 2011 A statistical framework for the prediction of fault-proneness *Adv. Mach. Learn. Appl. Softw. Eng.* **2011** 237–63

[42] Yücelbaş C, Yücelbaş Ş, Özşen S, Tezel G, Küççüktürk S and Yosunkaya Ş 2018 Automatic detection of sleep spindles with the use of STFT, EMD and DWT methods *Neural Comput. Appl.* **29** 17–33

[43] Yücelbaş Ş, Yücelbaş C, Tezel G, Özşen S and Yosunkaya Ş 2018 Automatic sleep staging based on SVD, VMD, HHT and morphological features of single-lead ECG signal *Expert Syst. Appl.* 102 193–206

[44] Yücelbaş C, Yücelbaş Ş, Özşen S, Tezel G, Küççüktürk S and Yosunkaya Ş 2018 A novel system for automatic detection of K-complexes in sleep EEG *Neural Comput. Appl.* **29** 137– 57